ences—Zn atoms locally destroy superconductivity[9] while Ni atoms do not.

Finally, magnetic probes sensitive to spin fluctuations reveal marked changes with Zn-doping[24,26–31] but only weak perturbations with Ni-doping[24,25,29,31]. Explanations for these phenomena have been proposed[5,6,27,28,30] whereby Zn behaves like a 'magnetic hole' (a spinless site in an environment of strongly exchange-coupled spins) that strongly alters NN exchange correlations and disrupts superconductivity, whereas Ni retains a magnetic moment that barely perturbs the antiferromagnetic exchange correlations that facilitate superconductivity. Although the NMR and INS data[24–31] are quite consistent with the magnetic component of such models, their predictions for local electronic phenomena at Ni and Zn can only now be tested for the first time. The STM data show that, despite their magnetic moments, scattering at Ni atoms is dominated by potential interactions. Furthermore, whereas Zn atoms locally destroy superconductivity within a 15 Å radius[9], the magnetic Ni atoms coexist with unweakened superconductivity. All these phenomena are consistent with the above proposals.

The resilience of cuprate-oxide high-T_c superconductivity against what should be the destructive effects of a magnetic impurity atom, and its concomitant vulnerability to destruction by a 'magnetic hole', are remarkable. These atomic-scale phenomena are now (through a combination of NMR, μSR and STM) coming into much clearer focus. They point towards a new approach to studying HTSC in which microscopic theories can be tested against an atomically resolved knowledge of impurity-state phenomena. □

Received 8 January; accepted 3 April 2001.

1. Abrikosov, A. A. & Gorkov, L. P. Contribution to the theory of superconducting alloys with paramagnetic impurities. *Sov. Phys. JETP* **12,** 1243–1253 (1961).
2. Monthoux, P., Balatsky, A. V. & Pines, D. Weak-coupling theory of high-temperature superconductivity in the antiferromagnetically correlated copper oxides. *Phys. Rev. B* **46,** 14803–14817 (1992).
3. Moriya, T., Takehashi, Y. & Ueda, K. Antiferromagnetic spin fluctuations and superconductivity in two-dimensional metals—a possible model for high T_C oxides. *J. Phys. Soc. Jpn* **59,** 2905–2915 (1990).
4. Bickers, N. E., Scalapino, D. J. & White, S. R. Conserving approximations for strongly correlated electron systems: Bethe-Salpeter equation and dynamics for the two-dimensional Hubbard model. *Phys. Rev. Lett.* **62,** 961–964 (1989).
5. Monthoux, P. & Pines, D. Spin-fluctuation-induced superconductivity and normal-state properties of $YBa_2Cu_3O_7$. *Phys. Rev. B* **49,** 4261–4278 (1994).
6. Pines, D. Understanding high temperature superconductors: progress and prospects. *Physica C* **282–287,** 273–278 (1997).
7. Balatsky, A. V., Salkola, M. I. & Rosengren, A. Impurity-induced virtual bound states in d-wave superconductors. *Phys. Rev. B* **51,** 15547–15551 (1995).
8. Salkola, M. I., Balatsky, A. V. & Schrieffer, J. R. Spectral properties of quasiparticle excitations induced by magnetic moments in superconductors. *Phys. Rev. B* **55,** 12648–12661 (1997).
9. Pan, S. H. *et al.* Imaging the effects of individual zinc impurity atoms on superconductivity in $Bi_2Sr_2CaCu_2O_{8+\delta}$. *Nature* **403,** 746–750 (2000).
10. Mendels, P. *et al.* Macroscopic magnetic properties of Ni and Zn substituted $YBa_2Cu_3O_x$. *Physica C* **235/240,** 1595–1596 (1994).
11. Salkola, M. I., Balatsky, A. V. & Scalapino, D. J. Theory of scanning tunneling microscopy probe of impurity states in a d-wave superconductor. *Phys. Rev. Lett.* **77,** 1841–1844 (1996).
12. Flatté, M. E. & Byers, J. M. Impurity effects on quasiparticle c-axis planar tunneling and STM spectra in high-Tc cuprates. *Phys. Rev. Lett.* **80,** 4546–4549 (1998).
13. Tsuchiura, H., Tanaka, Y., Ogata, M. & Kashiwaya, S. Local density of states around a magnetic impurity in high-T_C superconductors based on the t-J model. *Phys. Rev. Lett.* **84,** 3165–3168 (2000).
14. Flatté, M. E. Quasiparticle resonant states as a probe of short-range electronic structure and Andreév coherence. *Phys. Rev. B* **61,** R14920–14923 (2000).
15. Haas, S. & Maki, K. Quasiparticle bound states around impurities in $d_{x^2-y^2}$-wave superconductors. *Phys. Rev. Lett.* **85,** 2172–2175 (2000).
16. Martin, I., Balatsky, A. V. & Zaanen, J. Impurity states and interlayer tunneling in high temperature superconductors. Preprint cond-mat/0012446 at <xxx.lanl.gov> (2000).
17. Zhang, G.-M., Hu, H. & Yu, L. Marginal Fermi liquid resonance induced by quantum magnetic impurity in d-wave superconductors. *Phys. Rev. Lett.* **86,** 704–707 (2001).
18. Yazdani, A., Howald, C. M., Lutz, C. P., Kapitulnik, A. & Eigler, D. M. Impurity-induced bound excitations on the surface of $Bi_2Sr_2CaCu_2O_8$. *Phys. Rev. Lett.* **83,** 176–179 (1999).
19. Yazdani, A., Jones, B. A., Lutz, C. P., Crommie, M. F. & Eigler, D. M. Probing the local effects of magnetic impurities on superconductivity. *Science* **275,** 1767–1770 (1997).
20. Flatté, M. E. & Byers, J. M. Local electronic structure of a single magnetic impurity in a superconductor. *Phys. Rev. Lett.* **78,** 3761–3764 (1997).
21. Maeda, A., Yabe, T., Takebayashi, S., Hase, M. & Uchinokura, K. Substitution of 3d metals for Cu in $Bi_2(Sr_{0.6}Ca_{0.4})_3Cu_2O_y$. *Phys. Rev. B* **41,** 4112–4117 (1990).
22. Kuo, Y. K. *et al.* Effect of magnetic and nonmagnetic impurities (Ni,Zn) substitution for Cu in $Bi_2(SrCa)_{2+n}(Cu_{1-x}M_x)_{1+n}O_y$ whiskers. *Phys. Rev. B* **56,** 6201–6206 (1997).
23. Bonn, D. A. *et al.* Comparison of the influence of Ni and Zn impurities on the electromagnetic properties of $YBa_2Cu_3O_{6.95}$. *Phys. Rev. B* **50,** 4051–4063 (1994).
24. Ishida, K. *et al.* Cu NMR and NQR studies of impurities-doped $YBa_2(Cu_{1-x}M_x)_3O_7$ (M=Zn and Ni). *J. Phys. Soc. Jpn* **62,** 2803–2818 (1993).
25. Tokunaga, Y., Ishida, K., Kitaoka, Y. & Asayama, K. Novel relation between spin-fluctuation and superconductivity in Ni substituted high-T_C cuprate $YBa_2Cu_3O_7$: Cu NQR study. *Solid State Comm.* **103,** 43–47 (1997).
26. Mahajan, A. V., Alloul, H., Collin, G. & Marucco, J. F. ^{89}Y NMR probe of Zn induced local moments in $YBa_2(Cu_{1-y}Zn_y)_3O_{6+x}$. *Phys. Rev. Lett.* **72,** 3100–3103 (1994).
27. Bobroff, J. *et al.* Spinless impurities in high-T_C cuprates: Kondo-like behavior. *Phys. Rev. Lett.* **83,** 4381–4384 (1999).
28. Bobroff, J. *et al.* Persistence of Li induced Kondo moments in the superconducting state of cuprates. *Phys. Rev. Lett.* **86,** 4116–4119 (2001).
29. Williams, G. V. M., Tallon, J. L. & Dupree, R. NMR study of magnetic and non-magnetic impurities in $YBa_2Cu_4O_8$. *Phys. Rev. B* **61,** 4319–4325 (2000).
30. Julien, M.-H. *et al.* ^{63}Cu NMR evidence for enhanced antiferromagnetic correlations around Zn impurities in $YBa_2Cu_3O_{6.7}$. *Phys. Rev. Lett.* **84,** 3422–3425 (2000).
31. Sidis, Y. *et al.* Quantum impurities and the neutron resonance peak in $YBa_2Cu_3O_7$: Ni versus Zn. *Phys. Rev. Lett.* **84,** 5900–5903 (2000).
32. Bernhard, C. *et al.* Suppression of the superconducting condensate in the high-T_C cuprates by Zn substitution and overdoping: Evidence for an unconventional pairing state. *Phys. Rev. Lett.* **77,** 2304–2307 (1996).

Acknowledgements

We acknowledge H. Alloul, P. W. Anderson, A. V. Balatsky, D. Bonn, M. Flatté, M. Franz, D.-H. Lee, K. Maki, I. Martin, P. Monthoux, A. Mourachkine, D. Pines, D. Rokhsar, S. Sachdev, D. J. Scalapino and A. Yazdani for conversations and communications, and J. E. Hoffman for help with data analysis. Support was from the Office of Naval Research, the Department of Energy through an LDRD from LBNL, the UCDRD Program, Grant-in-Aid for Scientific Research on Priority Area (Japan), a COE Grant from the Ministry of Education, Japan, the Miller Inst. for Basic Research (J.C.D.), and by the IBM Graduate Fellowship Program (K.M.L.).

Correspondence and requests for materials should be addressed to J.C.D. (e-mail: jcdavis@physics.berkeley.edu).

Liquid marbles

Pascale Aussillous & David Quéré

Laboratoire de Physique de la Matière Condensée, URA 792 du CNRS, Collège de France, 75231 Paris Cedex 05, France

The transport of a small amount of liquid on a solid is not a simple process, owing to the nature of the contact between the two phases. Setting a liquid droplet in motion requires non-negligible forces (because the contact-angle hysteresis generates a force opposing the motion[1]), and often results in the deposition of liquid behind the drop. Different methods of levitation—electrostatic, electromagnetic, acoustic[2], or even simpler aerodynamic[2,3] techniques—have been proposed to avoid this wetting problem, but all have proved to be rather cumbersome. Here we propose a simple alternative, which consists of encapsulating an aqueous liquid droplet with a hydrophobic powder. The resulting 'liquid marbles' are found to behave like a soft solid, and show dramatically reduced adhesion to a solid surface. As a result, motion can be generated using gravitational, electrical and magnetic fields. Moreover, because the viscous friction associated with motion is very small[4], we can achieve quick displacements of the droplets without any leaks. All of these features are of potential benefit in microfluidic applications, and also permit the study of a drop in a non-wetting situation—an issue of renewed interest following the recent achievement of super-hydrophobic substrates[5].

Liquid marbles are obtained by making a small amount of liquid (typically between 1 and 10 mm^3) roll in a very hydrophobic powder (we used lycopodium grains of typical size 20 μm covered with fluorinated silanes). The grains spontaneously coat the drop, which can eventually be transferred onto other substrates. Figure 1 shows a marble of radius 1 mm, made of water and put on a glass plate (which would be wetted by water), where it is observed to adopt a spherical shape. Thanks to the monolayer of grains at the liquid–air interface, the wetting between the glass and the water is suppressed.

The marble can even be transferred onto a water pool, on which it is observed to float. Here we discuss the statics and dynamics of these marbles. By using mixtures of water and glycerol, the liquid viscosity was varied over a large range (a factor of 10^3), which allows us to describe the viscous and inertial dynamical regimes.

We first consider the size l of the contact between the marble and the solid. If there were a contact angle θ between the solid and the liquid (as usually occurs), l would be given by a simple geometric relation: $l = R\sin\theta$, where R is the radius of the droplet. Thus, l should tend to zero for non-wetting liquids ($\theta = 180°$). However, the weight of the droplet needs to be considered[4]: the exact shape of the drop results from a balance between gravity (which favours a contact) and capillarity (which opposes it, because of the deformation it induces)[4]. If the centre of mass is lowered by a quantity δ, the difference in energy from a sphere tangent to the plane can be written dimensionally as: $\Delta E \approx \gamma\delta^2 - \rho g R^3\delta$. Minimization of this expression yields δ, and thus, using the geometric relation $l^2 \approx \delta R$:

$$l \approx R^2\kappa \qquad (1)$$

where κ^{-1} is the capillary length ($\kappa^{-1} = \sqrt{\gamma/\rho g}$, where γ and ρ are, respectively, the liquid surface tension and the density). If the Laplace equation is solved numerically, the contact size can be plotted as a function of the drop radius. It is indeed found to be quadratic in R, with a numerical coefficient of the order of 0.8 (M. Perez, personal communication). For drops of initial radius R larger than the capillary length, gravity flattens the drop into a puddle. As the thickness of the puddle is fixed by gravity and surface tension, it must scale with the capillary length[6]. By invoking conservation of liquid volume, we can obtain the scaling law for the contact size: $l \approx R^{3/2}\kappa^{1/2}$.

A liquid marble indeed develops a contact with its substrate (Fig. 1). We measured the contact size l as a function of the drop radius, for two different powders (the lycopodium mentioned above, and a silanized silica powder of size ~100 nm) and two kinds of substrate (glass and Teflon plates). The results are displayed in Fig. 2a, where the data are found to collapse onto two curves. (1) For small droplets ($R < \kappa^{-1}$), the contact size indeed scales as R^2, as predicted by equation (1), which proves that the contact is not a classical wetting one; the numerical coefficient is found to be 0.9, in close agreement with the numerical simulations. (2) Larger drops ($R > \kappa^{-1}$) form puddles, which yields the scaling behaviour in $R^{3/2}$.

We now consider the movement of such marbles on an inclined plane. We restrict our studies to the case of marbles formed from rather viscous liquids (viscosity $\eta > 200$ mPa s), in order to stress the small friction, related to the non-wetting, and the unusual laws of dissipation it generates. The motions are found to be stationary after a short while (constant descent velocity, no liquid film remaining behind the drops). Thanks to the powder at the liquid–air interface, we can see that the marbles roll as they move.

The first series of experiments were performed with a small slope α (less than 10°). Usually, droplets would remain stationary in such a low field (~0.1g), because of contact-angle hysteresis[1]. In contrast, we found descent velocities that were rather large (of the order of 1 cm s^{-1}), even for very viscous fluids (~1,000 mPa s). In Fig. 2b, this velocity is plotted as a function of the droplet radius. The velocity and drop size are respectively normalized by the puddle velocity V_o (which should be independent of the puddle size) and by the capillary length κ^{-1}. Because of the normalization, all the data lie on the same curve. (1) For large drops (puddles), the velocity is indeed found to be independent of the drop size. It results from a balance between viscous friction and gravity. Because the puddle thickness is also independent of the drop size and fixed at a value of $2\kappa^{-1}$ (the maximum gravity pancake thickness, reached for an angle $\theta = 180°$)[6], the puddle velocity can be derived[7]: $V_o \approx \gamma/\eta \sin\alpha$, which is drawn in Fig. 2b (the horizontal straight line), and found to fit the data. (2) For small droplets, the velocity increases when the drop size is decreased, which implies a very unusual friction law. This behaviour was recently predicted by Mahadevan and Pomeau[4], and observed to apply qualitatively to droplets running down a so-called super-hydrophobic plate[7]. In the limit of small Reynolds numbers, Mahadevan and Pomeau[4] propose that the droplet motion can be described as a superposition of a solid rotation (producing no dissipation) and a viscous friction localized in the contact zone.

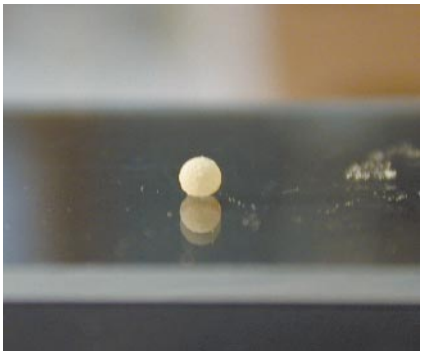

Figure 1 A liquid marble. Water is mixed with a very hydrophobic powder (silane-treated lycopodium grains of typical size 20 μm). The powder spontaneously migrates to the water–air interface, and thus protects the water, which then behaves as if it were perfectly non-wetting when transferred on a glass plate. (Drop radius, 1 mm.)

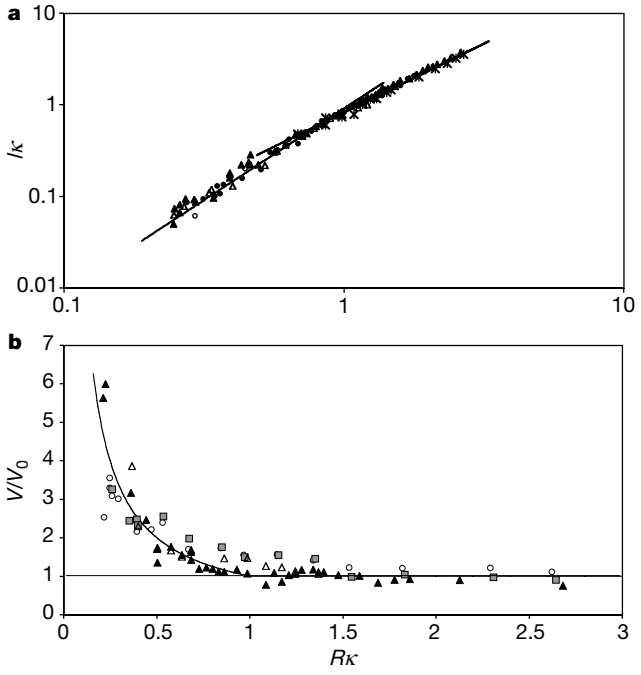

Figure 2 Contact of static liquid marbles, and their velocity on slightly tilted plates. **a**, The radius (l) of the contact between marble and substrate plotted against the radius (R) of the spherical drop. Both are normalized by the capillary length $\kappa^{-1} = (\gamma/\rho g)^{1/2}$. Lycopodium grains or silica were used as coating powders (represented by filled and open symbols, respectively). The liquid can be either water (triangles) or glycerol (circles). The marbles are deposited on glass, except in one case where glycerol was deposited on Teflon (stars). The straight lines represent slope 2 (equation (1)) and 1.5. **b**, Drop velocity (V) normalized by the puddle velocity (V_0) plotted against the drop radius (R) normalized by the capillary length (κ^{-1}), for different liquid viscosities, η, and slopes, α: open circles, $\eta = 270$ mPa s, $\alpha = 5°$; grey squares, $\eta = 450$ mPa s, $\alpha = 5°$; filled triangles, $\eta = 1{,}150$ mPa s, $\alpha = 4°$; open triangles, $\eta = 1{,}150$ mPa s, $\alpha = 8°$. The hyperbola is derived from equation (2), with 1 as a numerical constant.

Droplet deformation is small at low velocity, so that the size of this zone remains given by the static law (equation (1)). Typical velocity gradients in the drop are of the order of V/R, and the viscous force can be dimensionally written as: $f \approx \eta V/Rl^2$. Balancing the torque fl associated with this force by the gravity torque $\rho g R^4$ yields the marble velocity[4]:

$$V \approx V_0 \frac{\kappa^{-1}}{R} \qquad (2)$$

As shown in Fig. 2b, such a hyperbolic law is found to fit the data fairly well, taking a numerical coefficient of the order of 1. This confirms that the hydrodynamics associated with these liquid marbles is very unusual, mainly because of the absence of a contact line. From a practical point of view, we stress that by dressing a drop with a hydrophobic powder, a weak field can drive the drop to a rather high speed (and higher if the drop is small).

The model of ref. 4 should be valid provided that the drop keeps a quasi-static shape, where inertial and viscous forces do not deform the spherical shape. This requires that both the Weber ($\rho V^2 R/\gamma$) and the capillary ($\eta V/\gamma$) numbers, which compare inertia and viscous force with surface tension, respectively, are less than unity. Together with the condition of small Reynolds number, this implies that the drop must be large enough ($R > \kappa^{-1}\sin\alpha$) and the liquid viscous enough ($\eta > (\gamma\rho\kappa^{-1}\sin\alpha)^{1/2}$). These conditions are fulfilled in the series of experiments displayed in Fig. 2b. We were interested in observing what happened when the influence of inertia was increased: this was examined by tilting the plate more (which generates larger velocities).

Figure 3 compares what happens when using a viscous marble on a small slope and on a greater slope ($\alpha = 4°$ and $\alpha = 24°$). Again, the velocity (scaled by the puddle velocity) is plotted versus the drop radius, and compared with the model of ref. 4 (equation (2)). A very large deviation is observed when the plate slope is increased, which reveals a regime of much smaller friction. The high velocities that are obtained (of the order of 1 m s^{-1}) induce strong deformations in the drop, as shown in Fig. 4, where successive snapshots of the drop (obtained with a high-speed camera) are displayed.

Two kinds of shape are observed, which can be both related to the action of centrifugal force. (1) A peanut shape, which has also been observed for drops rotating in space[8,9], and which has been discussed theoretically[10,11]. (2) A more unusual deformation, which conserves the axial symmetry of the drop: as it accelerates, it gradually passes from a sphere to a disk, and eventually to a doughnut (toroidal) shape. The light intensity for a horizontal section crossing all the 'doughnut' centres is drawn in Fig. 4c. It may be seen that the 'holes' in the 'doughnuts' are not totally black. This means that the 'doughnut' is not fully open—opening could be delayed by the viscous drainage in the thin zone, around the centre of the doughnut, and implies the nucleation of a hole).

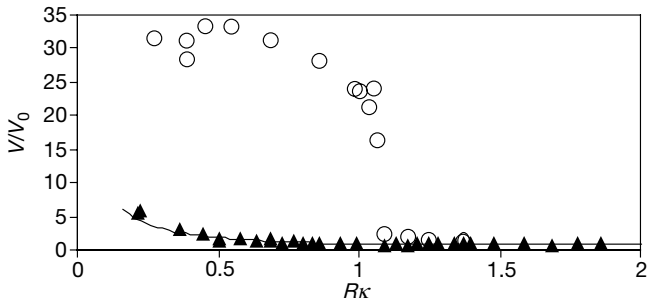

Figure 3 Comparison of the mobility of a liquid marble on two different slopes. The velocity V of viscous ($\eta = 1{,}150$ mPa s) marbles (scaled by the puddle velocity V_0) is plotted against their radius R (scaled by the capillary length κ^{-1}), for $\alpha = 4°$ (triangles) and $\alpha = 24°$ (circles). The full line corresponds to equation (2).

A toroidal shape for a revolving drop has been proposed[12] and discussed[10]; but to the best of our knowledge such a shape has not been previously observed. (The formation of a torus has been reported when a very viscous liquid drop, held by a fibre inside another liquid of the same density, was rotated—which seems to be a different experiment[13]). The torus is claimed to be unstable compared with the peanut shape[10,14]; its stability here seems to be promoted by the presence of an inclined plane below the marble. If this plane is removed (which may done by putting an obstacle like a needle in the path of the drop, or more simply by observing what happens beyond the extremity of the plane), the axisymmetric shape evolves towards the peanut shape. This is illustrated in Fig. 4d. More generally, the torus seems to be metastable, and often evolves towards a peanut shape during its descent, usually because a small eccentricity in its shape makes it take off. A quantitative description of these different shapes, together with a comprehensive analysis of this low-friction regime, remains to be made.

Liquid marbles thus seem to be an interesting solution to the problem of driving small amounts of liquid on solid (or even liquid) substrates. In the present work we used gravity as a field to move the drop; but we have found that other weak fields (such as electric or magnetic fields) also drive liquid marbles (data not shown). Understanding the shape changes that we have observed will require the derivation of a friction law that takes shape evolution into account. We are at present examining the notable robustness of these marbles, which are able to resist a series of shocks (such as those observed in Fig. 4a). □

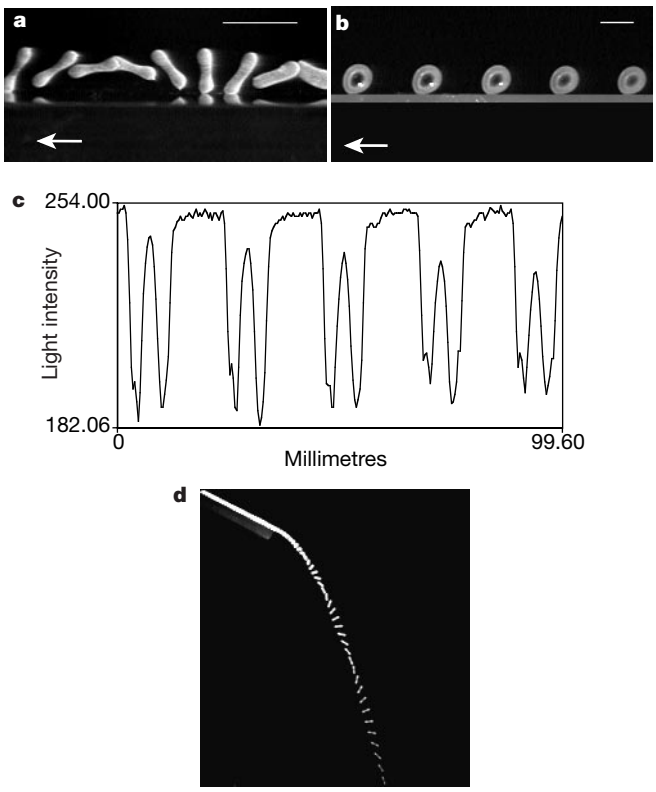

Figure 4 Different shapes taken by a liquid marble in the inertial regime. In pictures **a** and **b**, both the camera and the plane are tilted. Arrow, direction of the motion; scale bar, 1 cm. **a**, $\alpha = 34°$, $R = 1.3$ mm, interval between two pictures, 9 ms; **b**, $\alpha = 36°$, $R = 2.5$ mm, interval between two pictures, 23 ms. **c**, Light intensity for a horizontal section crossing all the 'doughnut' centres of **b**; 255 means black, and 0 white. **d**, Successive snapshots (interval between each, 6.7 ms) showing the evolution of an axisymmetric liquid marble as it leaves an inclined plane. The marble spontaneously transforms into a peanut shape.

Received 19 February; accepted 5 April 2000.

1. Dussan, V. E. B. & Chow, R. T. P. On the ability of drops or bubbles to stick to non-horizontal surfaces of solids. *J. Fluid Mech.* **137,** 1–29 (1983).
2. Frohn, A. & Roth, R. *Dynamics of Droplets* (Springer, Berlin, 2000).
3. Perez, M. *et al.* Oscillation of liquid drops under gravity: influence of shape on the resonance frequency. *Europhys. Lett.* **47,** 189–195 (1999).
4. Mahadevan, L. & Pomeau, Y. Rolling droplets. *Phys. Fluids* **11,** 2449–2453 (1999).
5. Onda, T., Shibuichi, S., Satoh, N. & Tsujii, K. Super water-repellent fractal surfaces. *Langmuir* **12,** 2125–2127 (1996).
6. Taylor, G. I. & Michael, D. H. On making holes in a sheet of fluid. *J. Fluid Mech.* **58,** 625–639 (1973).
7. Richard, D. & Quéré, D. Drops rolling on a tilted non-wettable solid. *Europhys. Lett.* **48,** 286–291(1999).
8. Wang, T. G. *et al.* Bifurcation of rotating liquid drops: results from USML-1 experiments in space. *J. Fluid Mech.* **276,** 389–403 (1994).
9. Lee, C. P. *et al.* Equilibrium of liquid drops under the effects of rotation and acoustic flattening: results from USML-2 experiments in space. *J. Fluid Mech.* **354,** 43–67 (1998).
10. Brown, R. A. & Scriven, L. E. The shape and stability of rotating liquid drops. *Proc. R. Soc. Lond. A* **371,** 351–367 (1980).
11. Brown, R. A. & Scriven, L. E. New class of asymmetric shapes of rotating liquid drops. *Phys. Rev. Lett.* **45,** 180–183 (1980).
12. Rayleigh, Lord The equilibrium of revolving liquid under capillary force. *Phil. Mag.* **28,** 161–170 (1914).
13. Plateau, J. A. F. Experimental and theoretical researches on the figures of equilibrium of a liquid mass withdrawn from the action of gravity. *Annu. Rep. Board Regents Smithson. Inst.* 207–285 (1863).
14. Chandrasekhar, S. The stability of a rotating liquid drop. *Proc. R. Soc. Lond A* **286,** 1–26 (1965).

Acknowledgements

We thank J. Bico and D. Richard for silanization of lycopodium grains and the achievement of a first series of liquid marbles, C. Clanet for help with high-speed pictures and for discussions, and P.-G. de Gennes for discussions and encouragement.

Correspondence and requests for materials should be addressed to D.Q. (e-mail: quere@ext.jussieu.fr).

Decreasing overflow from the Nordic seas into the Atlantic Ocean through the Faroe Bank channel since 1950

Bogi Hansen*, William R. Turrell† & Svein Østerhus‡

** Faroese Fisheries Laboratory, PO Box 3051, FO-110 Tórshavn, Faroe Islands*
† FRS Marine Laboratory, PO Box 101, Aberdeen AB11 9DB, UK
‡ Bjerknes Centre for Climate Research and Geophysical Institute, N-5024 Bergen, Norway

The overflow of cold, dense water from the Nordic seas, across the Greenland–Scotland ridge[1] and into the Atlantic Ocean is the main source for the deep water of the North Atlantic Ocean[2]. This flow also helps drive the inflow of warm, saline surface water into the Nordic seas[1]. The Faroe Bank channel is the deepest path across the ridge, and the deep flow through this channel accounts for about one-third of the total overflow[1,2]. Previous work has demonstrated that the overflow has become warmer and less saline[3,4] over time. Here we show, using direct measurements and historical hydrographic data, that the volume flux of the Faroe Bank channel overflow has also decreased. Estimating the volume flux conservatively, we find a decrease by at least 20 per cent relative to 1950. If this reduction in deep flow from the Nordic seas is not compensated by increased flow from other sources, it implies a weakened global thermohaline circulation and reduced inflow of Atlantic water to the Nordic seas.

The Nordic seas and the Arctic Ocean are dominated by cold water below about 500 m depth—the typical sill depth of the Greenland–Scotland ridge (Fig. 1). The overflow of this water across the Greenland–Scotland ridge into the North Atlantic is the most important source for North Atlantic Deep Water (NADW), and any assessment of past or future variation in the global thermohaline circulation will depend critically on assessing the variation of this overflow. About half of the overflow passes through the Denmark Strait, while the rest crosses the ridge in the Iceland–Scotland region[2], mainly through the Faroese channels—consisting of the Faroe–Shetland channel leading to the Faroe Bank channel (Fig. 1b).

The Faroe Bank channel has a sill depth of around 840 m, and the deepest parts of the channel are constantly filled with cold overflow water flowing into the Atlantic with average velocities exceeding 1 m s^{-1} in the core (Fig. 2). Since November 1995, an upward-looking acoustic Doppler current profiler (ADCP) has been moored at the sill of the channel and has measured the velocity profile almost continuously. From these measurements, initiated in the 'Nordic WOCE' project, the flux of water colder than 3 °C was estimated[5] to be 1.9 Sv (1 Sv = 10^6 m^3 s^{-1}), which is fairly consistent with previous estimates[6,7]. This flux includes the overflow waters, but also some entrained Atlantic water. To avoid influence from the entrained water, we focus on the well defined overflow, colder than +0.3 °C and with densities (σ_t) in excess of 28.0. From November 1995 to June 2000, the ADCP measurements indicate a weakening of this overflow flux of 2–4% per year (Fig. 3), which is significantly different from zero ($P < 0.001$).

Direct current measurements give the most reliable estimate of the overflow flux through the Faroe Bank channel, but for information on long-term variations we are restricted to more indirect methods. Historical hydrographic data may be used for this purpose if they can be related to the overflow on a theoretically sound basis. In the

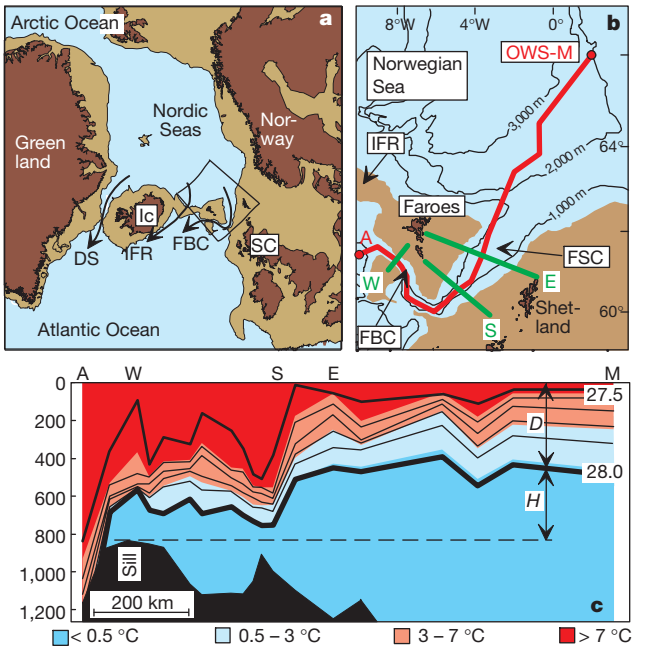

Figure 1 Topography and temperature change across the Greenland–Scotland ridge (light-brown areas are shallower than 500 m). **a**, Map of the Greenland–Iceland (Ic)–Scotland (Sc) region. Black arrows show overflow paths through the Denmark Strait (DS), over the Iceland–Faroe ridge (IFR), and through the Faroe Bank channel (FBC). **b**, Bottom topography of the study area (indicated by box in **a**) and location of a longitudinal (red line from A to OWS-M) and three transverse (green lines labelled W, S and E) standard hydrographic sections. Arrows indicate the Iceland–Faroe ridge (IFR), the Faroe–Shetland channel (FSC), and the Faroe Bank channel (FBC). **c**, Temperature (colour shading) and σ_t isopycnals (contours) along the longitudinal section, based on CTD (conductivity–temperature–depth) observations from RV *Magnus Heinason* in May–August 1991 and observations at OWS-M in the same period. The definition of the interface depth *D* and height *H* is illustrated.